pletely through the sedimentary layer in approximately 300 years.

A total of 59 measurements yielded 31 nonlinear temperature profiles (the rest are remarkably linear, to 0.005°C). Of these 31, 23 are in the survey areas 18×10^6 to 25×10^6 years old. Although the number of nonlinear temperature profiles appears to decrease with age, the flow rates through the sediments remain similar since the flow parameter β does not decrease with age. In addition, the amplitude of the heat flow pattern varies both between and within the survey areas. Since several hundred meters or more of insulating mud would be required to damp the temperature variation caused by the convection pattern in the oceanic crust, we conclude that the amplitude as well as the wavelength varies from cell to cell.

It had earlier been thought that convection within the oceanic crust might stop at ages corresponding to the transition from low to normal heat flow on the flanks of midoceanic ridges (*5*). This transition occurs in sea floor 40×10^6 to 60×10^6 years old in the Crozet and Madagascar basins (Fig. 4). Our heat flow measurements show large-amplitude, small-scale geothermal variations that can only be explained as the result of vigorous convective heat transfer in the oceanic crust. This circulation continues beyond the age of the transition from low to high heat flow. The presence of nonlinear temperature profiles in all of our survey areas is best explained as a result of convective heat transfer through the sediments in addition to vigorous convection in the oceanic crust. Convection between the crust and the ocean continues even when a uniform blanket of sediments 100 m thick is draped over the oceanic basement. This pervasive geothermal circulation through the sediments and within the oceanic crust will have major implications for the chemistry of the oceanic crust, sediments, and the ocean itself (*10*).

The mean heat flow, well below theoretical predictions, observed at the survey site 18×10^6 years old perhaps indicates that much of the convective heat transfer in the younger crust is being channeled through "chimneys" of rock outcropping through the irregular sedimentary cover and thus is bypassing the areas where we can measure the heat flow. These chimneys would be subject to more prolonged and intense alteration than the adjacent sea floor. This rather ad hoc hypothesis may also provide a good explanation for the striking local variability in the grade of metamorphic alteration of the oceanic crust at International Program of Ocean Drilling sites 417 and 418 in the Atlantic Ocean (*11*); hole 417A possibly drilled into an old chimney.

There appear to be two types of convective heat transfer occurring through the sea floor of the Indian Ocean. Type 1 probably implies the convective exchange of heat from the geothermal circulation system in the oceanic crust directly to the water column, perhaps by chimneys of outcropping basement. Until we develop new techniques to measure heat flow on exposed rock, areas characterized by type 1 convection will continue to be recognizable only because the total observed heat flow will be low relative to predictions from theoretical models. Our results suggest that type 1 convection is sealed by the deposition of a uniform sedimentary blanket sufficiently thick to cover all basement outcrops; a thickness of 40 m appears to be sufficient in survey area 2. Oceanic heat flow measurements in the sedimentary layer directly detect only type 2 convection, that occurring in the oceanic crust and flowing through the sedimentary layer. Type 2 convection can only be recognized when closely spaced and sufficiently detailed temperature profiles are obtained so that nonlinearity can be identified, β values determined, and horizontal variability mapped. Even then, only discharge areas of upwelling fluids will ordinarily have measurable β values (very thin sediments being required to show curvature in downwelling or recharge areas). Despite the fact that regional heat flow analyses in the past have not been able to measure either type 1 or type 2 convection (*5*), the predominance of low heat flow on the flanks of all midoceanic ridges suggests that geothermal convection similar to that shown above is presently active beneath one-third of all of the world's ocean floor.

ROGER N. ANDERSON
MICHAEL A. HOBART
MARCUS G. LANGSETH
Lamont-Doherty Geological Observatory of Columbia University, Palisades, New York 10964

References and Notes

1. J. G. Sclater, R. N. Anderson, M. L. Bell, *J. Geophys. Res.* **76**, 7888 (1971).
2. D. L. Williams, R. P. Von Herzen, J. G. Sclater, R. N. Anderson, *Geophys. J. R. Astron. Soc.* **38**, 587 (1974).
3. C. R. B. Lister, *ibid.* **26**, 515 (1972); J. G. Sclater, J. Crowe, R. N. Anderson, *J. Geophys. Res.* **81**, 2997 (1976).
4. R. N. Anderson and M. A. Hobart, *J. Geophys. Res.* **81**, 2868 (1976).
5. R. N. Anderson, M. G. Langseth, J. G. Sclater, *ibid.* **82**, 3391 (1977); B. M. Herman, M. G. Langseth, M. A. Hobart, *Tectonophysics* **41**, 61 (1977).
6. V. Kolla *et al.*, *Mar. Geol.* **21**, 171 (1976).
7. R. J. Ribando, K. E. Torrance, D. L. Turcotte, *J. Geophys. Res.* **81**, 3007 (1976).
8. J. D. Bredehoeft and I. S. Papadopulos, *Water Resour. Res.* **1** (No. 2), 325 (1965).
9. This error estimate is based upon an analysis in Appendix II of R. P. Von Herzen and R. N. Anderson, *Geophys. J. R. Astron. Soc.* **26**, 427 (1972).
10. See R. A. Kerr, *Science* **200**, 1138 (1978).
11. T. W. Donnelly *et al.*, *Geotimes* **22** (No. 6), 21 (1977); W. B. Bryan *et al.*, *ibid.*, No. 7/8, p. 22; M. F. J. Flower *et al.*, *ibid.*, No. 9, p. 20.
12. We thank Capt. P. Cunningham and the officers and crew of the R.V. *Vema* for making these observations possible under the most adverse conditions. This work was supported by NSF grants OCE 76-21794 and INT 76-82960. Lamont-Doherty Geological Observatory Contribution No. 2828.

15 September 1978; revised 2 February 1979

Stratospheric Wave Spectra Resembling Turbulence

Abstract. *Pollution effects on ozone raise the question of the significance of turbulence in vertical transport in the stratosphere. The aircraft in situ measurements of velocity fluctuations previously employed to estimate turbulence transport were, it is hypothesized, due to atmospheric waves, despite their classical turbulence spectrum. This new hypothesis implies that previous turbulence estimates are invalid. Experimental tests are suggested.*

The current international concern about stratospheric pollution (as well as oceanic pollution) gives practical importance to the question of vertical transport due to turbulence in stratified fluids. Turbulence in such media, which is due presumably to the Kelvin-Helmholtz shear instability (*1*, *2*), takes the form of thin, horizontal pancake-shaped layers. In the stratosphere these have a vertical thickness of order 200 m [see (*3*), temporarily omitting the last entry] and a horizontal extent of tens of kilometers.

One method of estimating vertical transport due to turbulence makes use of the power density spectrum of the turbulent velocity fluctuations (*4*). Figure 1 shows such spectra obtained by means of an instrumented U-2 aircraft flying through what was presumed to be a turbulent layer in the stratosphere (*5*). The shape of these curves roughly fits the well-known $-5/3$ law predicted by Kolmogorov (*6*). His theory, which is based on dimensional analysis, predicts that $\phi = \alpha\epsilon_0^{2/3}k^{-5/3}$ for the steady-state "inertial subrange" of turbulence where it acts like a conservative cascade; that is, "big whirls have little whirls that feed on their velocity, and little whirls have less-

0036-8075/79/0525-0832$00.75/0

er whirls, and so on to viscosity (in the molecular sense)," as Richardson's poem (*7*) eloquently put it. Here ϕ is the power density spectrum, ϵ_0 the dissipation rate, k the wave number, and α the dimensionless universal constant of order unity. To estimate K (the eddy diffusion coefficient for diffusion of scalar quantities) inside a turbulent layer, Lilly *et al.* (*4*) assumed steady-state inertial range turbulence with R_f, the flux Richardson number, equal to the critical value, 0.25. From the steady-state assumption $\epsilon_0 = P - B$, where P and B are the turbulence production rate and buoyancy dissipation rate, respectively: $P \equiv -K_M S^2$ and $B \equiv -K_H N_B^2$ where K_M and K_H are the eddy diffusion coefficients for momentum and heat (scalar) and S and N_B are the vertical shear of the mean horizontal velocity and the buoyancy frequency, respectively. Using $R_f \equiv B/P = 1/4$ and solving for K_H, they obtained $K_H = \beta\epsilon_0/3N_B^2$. Knowing N_B from temperature measurements and ϵ_0 from the spectra, they calculated K_H.

As can be seen from Fig. 1, the maximum wavelengths are of order 10 km. Such large scales are excluded from the inertial range, as can be seen from the following argument. The maximum wavelength of the inertial range is 0.1 (or less) times the "outer length" or shear layer (*8, 9*) thickness (of order 200 m in the present case). Thus if we compare 20 m, the maximum inertial range wavelength, to the 12-km wavelength of Fig. 1, we see a gap of three orders of magnitude. Thus we conclude that inertial range turbulence cannot explain these data.

It is of some scientific interest that this anomalous $-5/3$ spectrum of stratified turbulence has been observed on several previous occasions both in the troposphere (*9, 10*) and in the laboratory (*11*). To date, however, it has remained an unexplained mystery.

Since Kolmogorov turbulence theory and other presently available theories of turbulence do not seem helpful in explaining Fig. 1, I now turn to what appears to be the only remaining plausible alternative. This is one which features a prominent role for running atmospheric waves (in addition to some small-scale turbulence). I assume in the following that these waves are exclusively of the buoyancy or "gravity" type of internal waves. As will be further explained below, however, the concepts of waves and turbulence represent two idealized extremes of fluid motion. The first case involves no interaction or diffusion effects, whereas the second involves strong interaction and eddy diffusion. In the real world, motions anywhere between these two extremes exist. Fortunately, data analysis techniques allow all gradations of these motions to be assessed regarding the degree of turbulence or wavelike properties.

The last entry of (*3*) gives average turbulent layer thickness based on measurements by steep ascents and descents of a U-2 aircraft (*12*). The fluctuations were thus found to be absent outside a thickness of order 1 km. My explanation is that the U-2 actually measured fluctuations that were predominantly due to buoyancy waves which were trapped inside finite layers due to the combined effects of wind and buoyancy frequency variations with altitude (*13, 14*). (This

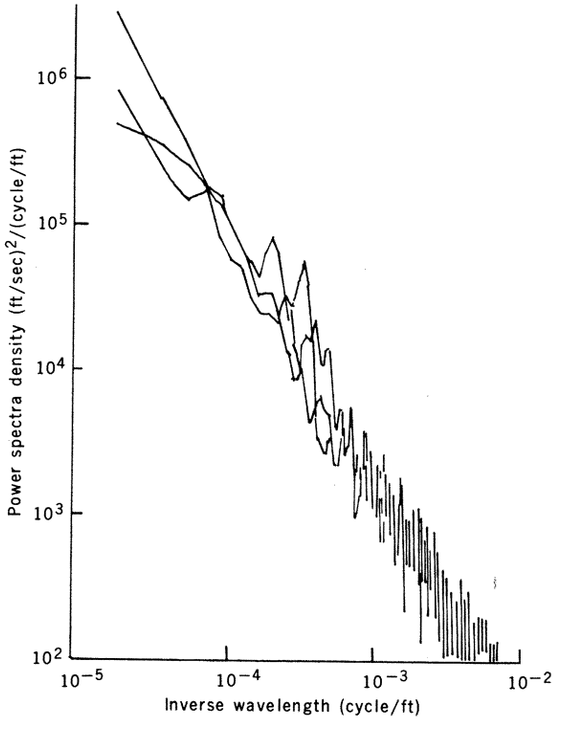

Fig. 1 (left). Power density spectrum of velocity fluctuations in the stratosphere measured in situ by instrumented U-2 aircraft, test 280, run 7 (*4*). Maximum wavelength is about 12.2 km. Fig. 2 (right). Energy equations decomposed into mean wave and turbulence scales (derived from the Navier-Stokes equations).

$$\frac{\partial E}{\partial t} = \boxed{A_1} - \frac{\partial}{\partial x_j}\left[E\bar{U}_j + \left(\frac{1}{\rho_0}\right)(\overline{P}\,\bar{U}_j) - \left(\frac{\nu}{2}\right)\frac{\partial E}{\partial x_j}\right] \boxed{D_{11}} - \bar{U}_i \frac{\partial}{\partial x_j}\left[\{\mathcal{U}_i \mathcal{U}_j\} + \{\langle u_i u_j\rangle\}\right] \boxed{D_{12}}$$

$$\boxed{C_1} - \nu\left(\frac{\partial \bar{U}_i}{\partial x_j}\frac{\bar{U}_i}{\partial x_j}\right) \qquad \boxed{B_1} - \bar{U}_i\, g\frac{\Theta}{\Theta_0}\,\delta_{i3} \tag{6}$$

$$\frac{\partial\{\xi\}}{\partial t} = \boxed{A_2} - \frac{\partial}{\partial x_j}\left[\bar{U}_j\{\xi\} + \{\mathcal{U}_j\xi\} + \left(\frac{1}{\bar{\rho}}\right)\{\rho\mathcal{U}_j\} - \left(\frac{\nu}{2}\right)\frac{\partial\{\xi\}}{\partial x_j}\right]$$

$$\boxed{D_2} - \left\{\mathcal{U}_i\frac{\partial\langle u_i u_j\rangle}{\partial x_j}\right\} \boxed{P_2} - \{\mathcal{U}_i\mathcal{U}_j\}\frac{\partial\bar{U}_i}{\partial x_j} \boxed{C_2} - \nu\left\{\frac{\partial\mathcal{U}_i}{\partial x_j}\frac{\partial\mathcal{U}_i}{\partial x_j}\right\}$$

$$\boxed{B_2} + \{\mathcal{U}_i\tilde{\theta}\}\frac{g}{\Theta_0}\delta_{i3} \tag{7}$$

$$\frac{\partial\langle e\rangle}{\partial t} = \boxed{A_3} - \frac{\partial}{\partial x_j}\left[(\bar{U}_j + \mathcal{U}_j)\langle e\rangle + \langle u_j e\rangle + \frac{\langle u_j p\rangle}{\bar{\rho}} - \left(\frac{\nu}{2}\right)\frac{\partial\langle e\rangle}{\partial x_j}\right]$$

$$\boxed{P_{31}} \boxed{P_{32}} - \langle u_j u_i\rangle\frac{\partial}{\partial x_j}\left[\mathcal{U}_i + \bar{U}_i\right] \boxed{B_3} + \frac{g}{\Theta_0}\langle\theta u_i\rangle\delta_{i3}$$

$$\boxed{C_3} - \nu\left\langle\frac{\partial u_i}{\partial x_j}\frac{\partial u_i}{\partial x_j}\right\rangle \tag{8}$$

"ducting" phenomenon is similar to effects seen in many other forms of wave propagation in stratified media, such as electromagnetic waves in natural waveguides in the ionosphere or acoustic waves in inversion layers in the ocean.) I propose furthermore that these waves "feed" an ensemble of turbulent layers within the trapped wave region by means of the shears that they generate at the crests and troughs. This phenomenon has already been observed and explained (*15, 16*) in the analogous case of the ocean, and already there is evidence for it in the atmosphere (*17, 18*).

Phillips (*16*) derived the following relation for the vertical shear of the mean wind due to a wave at crest and trough

$$\frac{d\mathcal{U}_1}{dX_3} = -\left(\frac{N_B^2}{\Omega^2} - 1\right)\Omega ka \qquad (1)$$

where $\mathcal{U}_1$ is the horizontal velocity due to the wave, X_3 the vertical coordinate, a the wave amplitude, and Ω the wave frequency. Physically, this shear is due to the tilt of the wave front. When $\Omega = N_B$, the fronts are vertical and $d\mathcal{U}_1/dX_3 = 0$.

The reverse process whereby a wave can be generated by means of a shear has been studied (*19-21*), and, as in the case of turbulence, the expression for the feeding of energy to the wave from the mean shear, $d\overline{U}_1/dX_3$ is given by

$$\frac{d\{\xi\}}{dt} = -\{\mathcal{U}_1\mathcal{U}_3\}\frac{d\overline{U}_1}{dX_3} \qquad (2)$$

where $\mathcal{U}_3$ is the vertical velocity of the fluid due to the wave, $\{\xi\}$ the average wave energy, and $\{\ \}$ an average explained below. Thus shear can feed waves and waves can cause shears. This suggests that there can be an energy cascade for a wave field.

To examine the flow of energy through spatial scales of waves and turbulence we start with the Navier-Stokes equations (*22, 23*)

$$\rho_0\frac{\partial U_i}{\partial t} + U_j\frac{\partial U_i}{\partial X_j} = \frac{\partial \Pi}{\partial X_i} + \mu\frac{\partial}{\partial X_j}\left(\frac{\partial U_i}{\partial X_j}\right) - \rho g\delta_{13} \qquad (3)$$

$$\frac{\partial U_j}{\partial X_j} = 0 \qquad (4)$$

where incompressibility and the Boussinesq approximation are assumed and U_i is the velocity components, Π the pressure, ρ_0 the average density of flow, g the acceleration of gravity, and μ the dynamic viscosity. Following Phillips (*16*) and Mollo-Christensen (*24*), we can use an extended form of Reynolds decomposition with spatial scales for mean, wave, and turbulence distances $L >> \mathcal{L} >> \ell$, respectively. The symbols $\{\ \}$ and $\langle\ \rangle$ represent averages over $\mathcal{L}$ and ℓ, respectively; $\{\mathcal{U}_i\} = 0$, $\langle u_i\rangle = 0$, $\langle\mathcal{U}_i\rangle = \mathcal{U}_i$, and so on (*24*). Thus

$$\begin{aligned}\rho &= \overline{\rho} + \tilde{\rho} + \rho_1\\ U_i &= \overline{U}_i + \mathcal{U}_i + u_i\\ \Pi &= \overline{P} + \mathcal{P} + p\end{aligned} \qquad (5)$$

where the first, second, and third terms refer to mean flow, waves, and turbulence, respectively, and when these are inserted into Eqs. 3 and 4, one obtains the result given in Fig. 2 [compare (*23, 24*)]. Here Θ_0 corresponds to the adiabatic lapse rate value, and $(\overline{U}_i\overline{U}_i)/2 \equiv E$, $\{\mathcal{U}_i\mathcal{U}_i\}/2 \equiv \{\xi\}$, and $\langle u_iu_i\rangle/2 \equiv \langle e\rangle$. The terms in Fig. 2 have been labeled to facilitate their physical identification. The subindices (or first subindices where there are two) 1, 2, 3 refer to the mean, wave, and turbulence levels, respectively. In particular, A stands for the divergence terms; D, the "scale drain" terms (*24*); C, viscous dissipation; P, production; and B, buoyancy dissipation through mixing. Note that the D and P terms form pairs that add into divergences. The A terms are divergences. When spatial integrals of these questions are taken over volumes such that the corresponding surfaces are all outside turbulent regions, then all divergences integrate to zero. Assuming a steady state for time intervals of interest, one may ignore the time derivatives. Assuming that D_{12}, P_{32}, B_2, C_1, and C_2 can be ignored (which should be the case physically), then from the above considerations (letting the labels stand now for the spatially integrated terms), $\epsilon_0 = C_3 = P_{31} - B_3$, $P_{31} = D_2 \equiv \epsilon'$, and therefore $\epsilon'(1 - R_f) = \epsilon_0$, where $R_f \equiv B_3/P_{31}$.

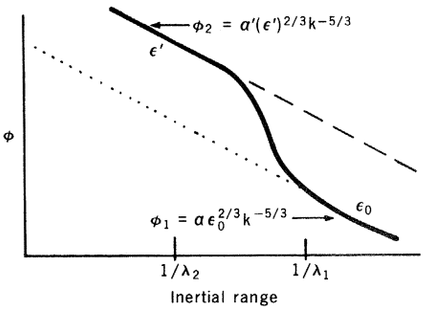

Fig. 3. The wave spectrum ϕ_2 depends on the wave dissipation rate, ϵ', and the turbulence spectrum ϕ_1 depends on the turbulent dissipation rate, ϵ_0. Wavelength λ_1 corresponds to the scale where dissipation to the turbulent velocity cascade becomes important, $\lambda_1 \sim (\epsilon_0 N_B^{-3})^{1/2}$, whereas $\lambda_2 >> (\epsilon' N_B^{-3})^{1/2}$; that is, the wave spectrum is found where negligible dissipation is taking place.

I now make the hypothesis that there is indeed a cascade of energy through the wave scales, and that this cascade is conservative and steady. In other words, I propose that "big waves have little waves that feed on deformation, and little waves have lesser waves to turbulent dissipation (in the eddy sense)." Such a cascade would differ fom the turbulent one both in the time constants and in the size of the jump in scale (being much larger in both for the wave case). With this postulate, one can simply follow Kolmogorov's dimensional argument, but in a new context, and insist that the spectrum $\phi \sim [L^3T^{-2}]$ depends only on $k \sim [L^{-1}]$ and on the rate of wave dissipation due to the energy given to turbulence by the wave-generated shears, $\epsilon' \sim [L^2T^{-3}]$. Thus $\phi = \alpha'(\epsilon')^{2/3}k^{-5/3}$. Figure 3 shows the form of the predicted spectrum for this situation. Both α' and α must be determined experimentally. The above considerations are easily extended to the turbulence spectrum for temperature fluctuations and will be discussed in a more extensive treatment (*25*).

To verify this theory, the following tests are proposed. The first is to use Stewart's method (*10*) to measure the ratio of wave to turbulence types of behavior via the cross spectrum between fluctuations of vertical velocity and temperature. Wavelike behavior is given by the quadrature spectrum and turbulent transport behavior by the cospectrum. The theory predicts wavelike behavior at the largest wavelengths. Axford (*26*) demonstrated the feasibility of this for atmospheric work. The second is to see if the prediction given by Fig. 3 is found at the higher k values. The third is to see if the stratospheric "turbulent layers" maintain constant altitude for long periods of time [see Crane's radar studies (*18*)]. The theory predicts that they will because the wind profiles (responsible for wave ducting) change very slowly in time (*27*). Clearly, if this prediction is correct, then values of K for small-scale turbulence (*4, 28*) may have to be revised downward by orders of magnitude since previous treatments assume random occurrence with altitude.

Finally, it should be noted that the Garrett-Munk spectrum (*29*) observed in the interior of the ocean may also turn out to be explained by the present model.

EDMOND M. DEWAN
Aeronomy Division, Air Force Geophysics Laboratory, Hanscom Air Force Base, Bedford, Massachusetts 01731

References and Notes

1. J. A. Dutton, *Rev. Geophys.* **9**, 613 (1971).
2. S. A. Thorpe, *Weather* **28**, 471 (Nov. 1973).
3. Turbulent layer vertical thickness measurements: balloon-borne sensor measurements, −200 m (*30*) and −200 m (*18*); estimate from Richardson number profiles, −160 m (*28*); vertical traverses of U-2 aircraft, −670 ± 580 m (*12*).
4. D. Lilly, D. Waco, S. Adelfang, *CIAP (Clim. Impact Assess. Program) Monogr. 1, DOT-TST-75-51* (1975), pp.6-81 to 6-90.
5. W. Crooks *et al.*, *Project HICAT (High Alt. Crit. Atmos. Turbul.) Rep. AD 847-497* (1968).
6. A. Kolmogorov, *C.R. (Dokl.) Acad. Sci. URSS* **31**, 538 (1941).
7. L. F. Richardson, *Weather Prediction by Numerical Process* (Cambridge Univ. Press, Cambridge, England, 1922).
8. H. Tennekes and J. L. Lumley, *A First Course in Turbulence* (MIT Press, Cambridge, Mass., 1972), chap. 8.
9. S. Pond, R. Stewart, R. Burling, *J. Atmos. Sci.* **20**, 319 (1963).
10. R. Stewart, *Radio Sci.* **4**, 1269 (1969).
11. Y.-H. Pao, *Bound-Layer Meteorol.* **5**, 177 (1973).
12. W. Crooks *et al.*, *Project HICAT AD 824-865* (1967).
13. I. Tolstoy, *Wave Propagation* (McGraw-Hill, New York, 1973), p. 105.
14. T. Beer, *Atmospheric Waves* (Wiley, New York, 1974), p. 120.
15. J. Woods and R. Wiley, *Deep-Sea Res. Oceanogr. Abstr.* **19**, 87 (1972).
16. O. Phillips, *The Dynamics of the Upper Ocean* (Cambridge Univ. Press, Cambridge, England, 1969), chaps. 4 and 5.
17. R. Stoeffler, *NASA Contract. Rep. CR-1985* (1972).
18. R. K. Crane, *U.S. Air Force Geophys. Lab. Rep. AFGL-TR-77-0207* (1977).
19. J. Miles, *J. Fluid Mech.* **3**, 185 (1957).
20. T. Brooke-Benjamin, *ibid.* **16**, 436 (1963).
21. B. Kinsman, *Wind Waves* (Prentice-Hall, Englewood Cliffs, N.J., 1965), chap. 11.
22. J. L. Lumley and H. A. Panofsky, *The Structure of Atmospheric Turbulence* (Interscience, New York, 1964), pp. 59-71.
23. J. T. Lin, S. Panchev, J. E. Cermak, "Turbulence spectra in the buoyancy subrange of thermally stratified shear flows" (Project Themis Tech. Rep. 1, College of Engineering, Colorado State Univ., Fort Collins, 1969), pp. 22-27.
24. E. Mollo-Christensen, *AIAA J.* **9**, 1217 (1971).
25. E. M. Dewan, in preparation.
26. D. Axford, *Q. J. R. Meteorol. Soc.* **97**, 313 (1971).
27. N. W. Rosenberg, R. E. Good, W. K. Vickery, E. M. Dewan, *AIAA J.* **12**, 1094 (1974).
28. N. W. Rosenberg and E. M. Dewan, *U.S. Air Force Cambridge Res. Lab. Rep. AFCRL-TR-75-0519* (1975).
29. C. Garrett and W. Munk, *Geophys. Fluid Dyn.* **2**, 225 (1972).
30. J. Barat, *C.R. Acad. Sci. Ser. B* **280**, 691 (1975).

31. I thank Chien-hsiung Yang for several helpful conversations.

16 October 1978; 27 March 1979

Effects of Raw Materials on Biface Manufacture

Abstract. *It has been suggested that the degree of refinement of trimming seen on Lower Paleolithic bifaces reflects the level of technical sophistication of the toolmaker. This has been tested by a series of experiments carried out at Olduvai Gorge, Tanzania, and related to some of the archeological assemblages there. It is concluded that advanced ideas and increased mastery over raw materials do not necessarily result in stone tools that are more refined in appearance.*

It is a widespread assumption among prehistorians that the refinement of trimming on Paleolithic bifaces (hand axes) as measured by the number of flake scars indicates the technical level of manufacture. There is also a consensus of opinion that such refinement can be used to compare different stone assemblages and thereby assess their chronological relationships (*1*-*3*). However, Mary Leakey has noted with reference to Olduvai: "It can be stated that there is no progressive trend, in the manufacture of bifaces, from Bed 11 to the Masek Beds, nor does the degree of trimming become more refined in the later occurrences" (*4*). Other workers have noticed a similar phenomenon on a continental basis (*5*).

In this report I attempt to describe how the nature of a raw material affects both the form of a stone tool made from it and the refinement of retouch evident on such a tool.

Bifaces occur at Olduvai in six main lithic materials: quartzite, basalt, trachyandesite, phonolite, nephelinite, and trachyte (*6*). I studied the flaking characteristics of these materials during several months of experimental biface manufacture at Olduvai. In all cases tool blank weight and dimensions were taken, manufacture time was recorded, all debitage was collected, and the finished tool was measured. Experiments were performed with particular emphasis on the kinds of biface blanks most probably used at Olduvai (lower and upper Bed IV). Raw materials were obtained from the sources used by the early occupants of the Olduvai area (*6*). Bifaces were made by direct freehand percussion with basalt hammerstones. The aim was to produce an efficient biface in as short a time as possible from each of the different types of blanks. The data on tool production shown in Fig. 1 indicate differences in production and activity level from typical blanks in each of the main raw material categories. Data are available for 20 to 30 bifaces and cleavers in each material (*7*).

Quartzite outcrops at Naibor Soit, a Precambrian inselberg about 3.5 km from the confluence of the Olduvai Main and Side gorges (see Fig. 2). This material is coarse-grained and generally white, although sometimes green (*6*). It occurs both in the main outcrop and in the form of detached chunks and tabular slabs, which litter the surrounding slopes. Tools can be made either from one of the slabs or from a large flake struck from the outcrop. The procedure used for biface production depends on whether the blank is a tabular slab or a large flake. A slab blank requires only to be flaked around its perimeter to give the tool sharp edges and the desired shape. Bifaces made from loose slabs often show the original tabular surfaces in the central part of each face. On the other hand, a large flake detached from the outcrop generally requires little trimming, as it already has sharp edges that can be incorporated as edges of the biface. When made in this way, quartzite bifaces are more often triangular in transverse section and thinner than those made from slabs.

When used for skinning and cutting meat, quartzite bifaces are very efficient, because the tool edges remain sharp during use and, when blunted, can be easily resharpened by removing a second series of flakes from the edge. Flakes are most easily detached by long, swinging, follow-through blows throughout production. The coarse grain of the quartzite inhibits the use of fine retouch.

Basalt and trachyandesite are from the volcano Lemagrut, 18 km south of Olduvai (Fig. 2). They are generally gray or almost black, vary from medium- to fine-grained, and are available in the form of water-rounded cobbles and boulders (*6*). The resilience of these materials and the sizes and shapes in which they occur require that large flakes be struck from the boulders to serve as biface blanks. Secondary flaking of these blanks is best carried out by means of large, swinging, follow-through blows that produce deeply indented but short flake scars. My experiments indicate that the unretouched edge of a large primary flake is sharper than the retouched edge. It is probably for this reason that most Olduvai bifaces made in basalt and trachyandesite incorporate these primary edges. The experiments have also shown that basalt bifaces are efficient when used for skinning and cutting meat, but that the primary flake edges cannot be resharpened effectively after becoming blunted. Basalt edges are more easily blunted than quartzite edges but last longer during use than phonolite edges.

Phonolite occurs at Engelosin, a steep-sided volcanic neck that outcrops about 12 km from the confluence of the gorges. It is very fine-grained material and generally dark green or gray in color (*6*). It occurs both in slabs and in large blocks on the slopes surrounding the outcrop.

Phonolite bifaces, like those of quartz-

0036-8075/79/0525-0835$00.50/0